Weierstraß-Institut

für Angewandte Analysis und Stochastik

Leibniz-Institut im Forschungsverbund Berlin e. V.

Preprint ISSN 2198-5855

Optimal and pressure-independent L^2 velocity error estimates for a modified Crouzeix-Raviart Stokes element with BDM reconstructions

Christian Brennecke[1], Alexander Linke[2], Christian Merdon[2] ,

Joachim Schöberl[3]

submitted: March 4, 2014

[1] Eidgenössische Technische Hochschule Zürich
Departement Mathematik
Ramistr. 101
8092 Zürich, Switzerland
email: cbrenne@student.ethz.ch

[2] Weierstrass Institute
Mohrenstr. 39
10117 Berlin
Germany
email: Alexander.Linke@wias-berlin.de
Christian.Merdon@wias-berlin.de

[3] Technische Universität Wien
Institut für Analysis und Scientific Computing
Wiedner Hauptstr. 8-10/101
1040 Wien, Austria
email: joachim.schoeberl@tuwien.ac.at

No. 1929

Berlin 2014

Key words and phrases. variational crime, Crouzeix-Raviart finite element, divergence-free mixed method, incompressible Navier-Stokes equations, a priori error estimates.

Edited by
Weierstraß-Institut für Angewandte Analysis und Stochastik (WIAS)
Leibniz-Institut im Forschungsverbund Berlin e. V.
Mohrenstraße 39
10117 Berlin
Germany

Fax: +49 30 20372-303
E-Mail: preprint@wias-berlin.de
World Wide Web: http://www.wias-berlin.de/

Abstract. Nearly all inf-sup stable mixed finite elements for the incompressible Stokes equations relax the divergence constraint. The price to pay is that a priori estimates for the velocity error become pressure-dependent, while *divergence-free* mixed finite elements deliver *pressure-independent* estimates. A recently introduced new variational crime using lowest-order Raviart-Thomas velocity reconstructions delivers a much more robust modified Crouzeix-Raviart element, obeying an optimal *pressure-independent* discrete H^1 velocity estimate. Refining this approach, a more sophisticated variational crime employing the lowest-order BDM element is proposed, which also allows proving an optimal pressure-independent L^2 *velocity error*. Numerical examples confirm the analysis and demonstrate the improved robustness in the Navier-Stokes case.

1. Introduction

The success of classical mixed finite elements for the incompressible Navier-Stokes equations relies heavily on the relaxation of the divergence constraint, enabling the construction of large classes of inf-sup stable finite element pairs for the approximation of velocity and pressure [BF91]. Unfortunately, this relaxation is not for free. In the simplest case, the incompressible Stokes equations

$$-\nu\Delta\mathbf{u} + \nabla p = \mathbf{f}, \quad \nabla\cdot\mathbf{u} = 0, \tag{1}$$

the classical a priori error estimate for the velocity error [BF91, GR86] reads (for homogeneous Dirichlet boundary conditions)

$$\|\mathbf{u}-\mathbf{u}_h\|_{1,h} \leqslant C_1 \inf_{\mathbf{w}\in X_h} \|\mathbf{u}-\mathbf{w}_h\|_{1,h} + \frac{C_2}{\nu} \inf_{q_h\in Q_h} \|p-q_h\|_0. \tag{2}$$

Divergence-free mixed finite element methods like the Scott-Vogelius finite element method deliver the *pressure-independent* and therefore significantly more robust estimate [GR86, BL08]

$$\|\mathbf{u}-\mathbf{u}_h\|_{1,h} \leqslant C_3 \inf_{\mathbf{w}\in X_h} \|\mathbf{u}-\mathbf{w}_h\|_{1,h}. \tag{3}$$

In many physical situations, where the pressure is comparably small w.r.t. the velocity or approximable by low-order polynomials, the appearance of the pressure in the estimate (2) is indeed negligible. In general situations, however, mixed methods suffer from so-called *poor mass conservation*. The easiest example, where mixed methods reveal their lack of robustness, is the *no-flow example* [DGT94, GLBB97, Lin08], where one prescribes $\mathbf{f} = \nabla\phi$ as the forcing in (1). For homogeneous Dirichlet boundary conditions, $(\mathbf{u}, p) = (\mathbf{0}, \phi)$ uniquely solves (1). Obviously, in this example the pressure $p = \phi$ is *not small* compared to the

Date: 4th March 2014.

Key words and phrases. variational crime, Crouzeix-Raviart finite element, divergence-free mixed method, incompressible Navier-Stokes equations, a priori error estimates.

velocity $\mathbf{u} = \mathbf{0}$. According to (3), divergence-free methods, deliver indeed a discrete velocity $\mathbf{u}_h = \mathbf{0}$, while mixed methods with a relaxed divergence constraint have a velocity error, which can be arbitrarily large, only dependent on ϕ, ν and the applied mixed method. Since the continuous velocity $\mathbf{u} = \mathbf{0}$ lies in the approximation space of the discrete method, mixed methods indeed suffer from a *stability problem*.

The traditional notion *poor mass conservation* is derived from conforming mixed methods like the Taylor-Hood element, where it is accompanied by large divergence errors. This numerical instability has been observed by several authors in the past. In [DGT94] the *no-flow* example was investigated for the first time, seemingly. In [GLBB97] a numerical Helmholtz decomposition of the forcing $\mathbf{f}$ in (1) was applied, in order to get around with the irrotational part of $\mathbf{f}$. The standard approach for stabilizing *poor mass conservation* is the so-called grad-div stabilization [FH88, OR04, OLHL09], which penalizes divergence errors in an L^2 sense. Unfortunately, it can be shown that even in the simplest case of the incompressible Stokes equations with an optimal choice of the stabilization parameter, the approach is not completely robust w.r.t. small kinematic viscosities ν [JJRL14]. More in the spirit of [GLBB97], recently in [Lin14] a new approach has been proposed, in order to avoid *poor mass conservation* completely. The approach is based on the observation that the proper source of the numerical instability is a *poor momentum balance*, where irrotational and divergence-free forces interact in a non-physical manner. Due to their L^2-orthogonality, divergence-free and irrotational forces are balanced separately in the continuous equations. But due to the relaxation of the divergence constraint in mixed methods, this separation fails in mixed methods, in general.

In [Lin14] it is shown how to reestablish L^2-orthogonality between discretely divergence-free and irrotational vector fields modifying the nonconforming Crouzeix-Raviart element [CR73] by a variational crime. Here, a velocity reconstruction operator maps *discretely divergence-free test functions* onto *divergence-free lowest-order Raviart-Thomas functions* [RT77] in the right hand side of the incompressible Stokes equations. Replacing the test functions by these reconstructions introduces an additional consistency error, but improves the robustness of the Crouzeix-Raviart element, since one can prove the *pressure-independent*, a priori discrete H^1 velocity error estimate (3) as done in [Lin14]. Unfortunately, in [Lin14] the author did not succeed in proving also an optimal a priori L^2 error estimate for the velocity, although numerical experiments show that such an estimate probably holds. The proof of an optimal L^2 velocity error is non-trivial, since divergence-free lowest-order Raviart-Thomas elements are piecewise constant, only, and the variational crime committed is similar to the replacement of an exact integration by a numerical quadrature.

In this contribution, a more sophisticated velocity reconstruction operator is introduced, which maps discretely divergence-free test functions onto divergence-free vector fields that are not only elementwise constant but elementwise affine, using the lowest order BDM element [BF91]. This allows an optimal pressure-independent a priori estimate for the velocity error in L^2.

The remaining parts of this paper are outlined as follows. Section 2 explains the continuous setting and its discretization with and without reconstructions. Section 3 proves a priori estimates for the energy error of the velocity and the L^2 error of the pressure. Section 4 proves an optimal L^2 error estimate for the reconstructions with BDM functions and sufficiently smooth exact solutions. Finally, Section 5 compares the modified Crouzeix-Raviart element with BDM and RT velocity reconstructions with the classical Crouzeix-Raviart element in four benchmark examples in order to verify the theoretical results.

2. Continuous and Discrete Setting

This section explains the continuous and the discrete setting for the model problem under consideration.

2.1. **Continuous setting.** Given the Sobolev spaces $V = H^1_0(\Omega)^d$, $H(\mathrm{div},\Omega)$ and $Q := L^2_0(\Omega)$, the weak solution $(\mathbf{u},p) \in V \times Q$ of the continuous steady incompressible Stokes and Navier-Stokes problems satisfies the equations

$$\begin{aligned} a(\mathbf{u},\mathbf{v}) + \gamma\, c(\mathbf{u},\mathbf{u},\mathbf{v}) + b(\mathbf{v},p) &= l(\mathbf{v}), \\ b(\mathbf{u},q) &= 0 \qquad \text{for all } (\mathbf{v},q) \in V \times Q \end{aligned} \tag{4}$$

with the multilinear forms defined by

$$\begin{aligned} a : V \times V \to \mathbb{R}, \qquad & a(\mathbf{u},\mathbf{v}) := \nu \int_\Omega \nabla\mathbf{u} : \nabla\mathbf{v}\, dx, \\ b : V \times Q \to \mathbb{R}, \qquad & b(\mathbf{u},q) := -\int_\Omega q \nabla\cdot\mathbf{u}\, dx, \\ c : V \times V \times V :\to \mathbb{R}, \qquad & c(\mathbf{a},\mathbf{u},\mathbf{v}) := \int_\Omega ((\mathbf{a}\cdot\nabla)\,\mathbf{u})\cdot\mathbf{v}\, dx, \\ l : V \to \mathbb{R}, \qquad & l(\mathbf{v}) := \int_\Omega \mathbf{f}\cdot\mathbf{v}. \end{aligned}$$

Within the set of weakly differentiable, divergence-free functions

$$V_0 := \{\mathbf{v} \in V : \nabla\cdot\mathbf{v} = 0\}, \tag{5}$$

the saddle point problem (4) becomes an elliptic problem for the velocity alone, i.e., $\mathbf{u} \in V_0$ such that

$$a(\mathbf{u},\mathbf{v}) + \gamma\, c(\mathbf{u},\mathbf{u},\mathbf{v}) = l(\mathbf{v}) \qquad \text{for all } \mathbf{v} \in V_0. \tag{6}$$

2.2. **Notation.** In the following, $\mathcal{T}$ denotes a regular triangulation of the domain Ω into triangles for $d = 2$ or tetrahedra for $d = 3$. For any element $T \in \mathcal{T}$, $\mathrm{mid}(T)$ denotes the barycenter of T. The set of all simplex faces, i.e., edges of triangles for $d = 2$ and faces of tetrahedra for $d = 3$, is denoted by $\mathcal{F}$. The subset $\mathcal{F}(\Omega)$ denotes the set of interior faces, while $\mathcal{F}(\partial\Omega)$ denotes the set of boundary faces along $\partial\Omega$. For any $F \in \mathcal{F}$, $\mathrm{mid}(F)$ denotes the barycenter of F and $\mathbf{n}_F$ abbreviates a face normal vector. The orientation of these normal vectors for the interior faces $F \in \mathcal{F}(\Omega)$ are arbitrary, but fixed. The normal vector $\mathbf{n}_F$ for boundary faces $F \in \mathcal{F}(\partial\Omega)$ points outwards of the domain Ω. For every simplex $T \in \mathcal{T}$, $\mathcal{F}(T)$ denotes the set of faces of this simplex and $\mathbf{n}_T$ denotes the outer normal of the simplex $T \in \mathcal{T}$. The function space of $P_k(\mathcal{T})$ contains piecewise polynomials of order k with respect to $\mathcal{T}$. For a piecewise Sobolev function $\mathbf{v} \in H^1(\mathcal{T})^d$ and some face $F \in \mathcal{F}(\Omega)$, the notion $[\mathbf{v}\cdot\mathbf{n}_F]$ denotes the jump of the normal flux over F, while $\{\{v\cdot\mathbf{n}_F\}\}$ denotes the average value of the normal flux over F. The space of Crouzeix-Raviart velocity trial functions is given by

$$\begin{aligned} \mathrm{CR}(\mathcal{T}) := \big\{ \mathbf{v}_h \in P_1(\mathcal{T})^d : \text{for all } T \in \mathcal{T},\ [\mathbf{v}_h](\mathrm{mid}(F)) = \mathbf{0} \text{ for all } F \in \mathcal{F}(\Omega) \\ \&\ \mathbf{v}_h(\mathrm{mid}(F)) = \mathbf{0} \text{ for all } F \in \mathcal{F}(\partial\Omega) \big\}. \end{aligned}$$

The pressure trial function space reads

$$Q(\mathcal{T}) := \left\{ q_h \in P_0(\mathcal{T}) : \int_\Omega q_h\, dx = 0 \right\}.$$

The space of Brezzi-Douglas-Marini finite element functions reads

$$\mathrm{BDM}(\mathcal{T}) := \quad \mathbf{v}_h \in P_1(\mathcal{T})^d : [\mathbf{v}_h \cdot \mathbf{n}_F] = 0 \text{ along all } F \in \mathcal{F}\Big\}.$$

Furthermore, consider its subspace of lowest order Raviart-Thomas finite element functions

$$\mathrm{RT}(\mathcal{T}) := \Big\{\mathbf{v}_h \in \mathrm{BDM}(\mathcal{T}) : \forall T \in \mathcal{T}\ \exists \mathbf{a}_T \in \mathbb{R}^d, b_T \in \mathbb{R},\ \mathbf{v}_h|_T(\mathbf{x}) = \mathbf{a}_T + b_T\mathbf{x}\Big\}.$$

The space $\mathrm{RT}(\mathcal{T})$ contains exactly the subset of functions with constant normal fluxes $\mathbf{v}\cdot\mathbf{n}_F \in P_0(F)$ on every face $F \in \mathcal{F}$ [BF91] and any Raviart-Thomas function is uniquely defined by its face normal fluxes at the face barycenters.

Remark 1. *A Crouzeix-Raviart function $\mathbf{v} \in \mathrm{CR}(\mathcal{T})$ is, in general, discontinuous along element faces $F \in \mathcal{F}$ except at the face barycenters. Therefore, $\mathrm{CR}(\mathcal{T}) \not\subset H(\mathrm{div}, \Omega)$ and $\mathrm{CR}(\mathcal{T}) \not\subset V_0$. On the contrary, $\mathrm{RT}(\mathcal{T}) \subset \mathrm{BDM}(\mathcal{T}) \subset H(\mathrm{div}, \Omega)$, because the normal components of any $\mathbf{v} \in \mathrm{RT}(\mathcal{T})$ or $\mathbf{v} \in \mathrm{BDM}(\mathcal{T})$ are continuous.*

The discrete setting employs the *broken gradient* $\nabla_h : \mathrm{CR}(\mathcal{T}) \to L^2(\Omega)^{d\times d}$ and the *broken divergence* $\nabla_h \cdot (\cdot) : \mathrm{CR}(\mathcal{T}) \to L^2(\Omega)$ in the sense that

$$(\nabla_h \mathbf{v}_h)|_T := \nabla(\mathbf{v}_h|_T), \quad (\nabla_h \cdot \mathbf{v}_h)|_T := \nabla \cdot (\mathbf{v}_h|_T) \quad \text{for all } T \in \mathcal{T}\,.$$

The discrete energy norm for the space $\mathrm{CR}(\mathcal{T})$ reads

$$\|\mathbf{v}_h\|_{1,h} := \left(\int_\Omega \nu \nabla_h \mathbf{v}_h : \nabla_h \mathbf{v}_h\, dx\right)^{1/2} = \|\nu^{1/2}\nabla_h \mathbf{v}_h\|_0. \tag{7}$$

2.3. **Interpolation operators.** The usual Crouzeix-Raviart interpolation operator $\boldsymbol{\pi}^{\mathrm{CR}} : V \to \mathrm{CR}(\mathcal{T})$ is defined by

$$(\boldsymbol{\pi}^{\mathrm{CR}}\,\mathbf{v})(\mathrm{mid}(F)) = \frac{1}{|F|}\int_F \mathbf{v}\, ds \quad \text{for all } F \in \mathcal{F}\,.$$

The Raviart-Thomas interpolation operator $\boldsymbol{\pi}^{\mathrm{RT}} : V \cup \mathrm{CR}(\mathcal{T}) \to \mathrm{RT}(\mathcal{T})$ is defined by

$$\mathbf{n}_F \cdot (\boldsymbol{\pi}^{\mathrm{RT}}\,\mathbf{v})(\mathrm{mid}(F)) = \frac{1}{|F|}\int_F \mathbf{v}\cdot\mathbf{n}_F\, ds \quad \text{for all } F \in \mathcal{F}\,.$$

Note that, due to continuity in the face barycenters, this is well-defined also for $\mathbf{v} \in \mathrm{CR}(\mathcal{T})$. Moreover, it holds the identity $\boldsymbol{\pi}^{\mathrm{RT}}\,\boldsymbol{\pi}^{\mathrm{CR}}\,\mathbf{v} = \boldsymbol{\pi}^{\mathrm{RT}}\,\mathbf{v}$ for any $\mathbf{v} \in V$.

We introduce a BDM interpolation operator $\boldsymbol{\pi}^{\mathrm{BDM}} : V \cup \mathrm{CR}(\mathcal{T}) \to \mathrm{BDM}(\mathcal{T})$ defined such that, for all $p_h \in P_1(F)$ on a face $F \in \mathcal{F}$,

$$\int_F (\boldsymbol{\pi}^{\mathrm{BDM}}\,\mathbf{v})\cdot\mathbf{n}_F\, p_h\, ds = \begin{cases} \int_F \{\{\mathbf{v}\cdot\mathbf{n_F}\}\}\, p_h\, ds & \text{for all } F \in \mathcal{F}(\Omega) \\ \int_F (\boldsymbol{\pi}^{\mathrm{RT}}\,\mathbf{v})\cdot\mathbf{n}_F\, p_h\, ds & \text{for all } F \in \mathcal{F}(\partial\Omega). \end{cases}$$

At the domain boundary $\partial\Omega$ the BDM interpolation equals the RT interpolation to ensure that $\boldsymbol{\pi}^{\mathrm{BDM}}\,\mathbf{v}_h \cdot \mathbf{n}$ for $\mathbf{v}_h \in \mathrm{CR}(\mathcal{T})$ vanishes along the complete boundary $\partial\Omega$. With this, the boundary integral in the integration by parts formula,

$$\int_\Omega (\boldsymbol{\pi}^{\mathrm{BDM}}\,\mathbf{v}_h)\nabla p\, dx = \int_\Omega \nabla\cdot(\boldsymbol{\pi}^{\mathrm{BDM}}\,\mathbf{v}_h) p\, dx + \int_{\partial\Omega} (\boldsymbol{\pi}^{\mathrm{BDM}}\,\mathbf{v}_h)\cdot\mathbf{n}\, p\, ds,$$

disappears and enables L^2-orthogonality of $\boldsymbol{\pi}^{\mathrm{BDM}}\,\mathbf{v}_h$ on gradients of all functions $p \in H^1(\Omega)$ for any discretely divergence-free $\mathbf{v}_h \in \mathrm{CR}(\mathcal{T})$. For any $\mathbf{v} \in V_0$, it immediately follows

$\nabla \cdot \boldsymbol{\pi}^{\mathrm{BDM}} \mathbf{v} = 0$, $\nabla \cdot \boldsymbol{\pi}^{\mathrm{RT}} \mathbf{v} = 0$ and $\nabla_h \cdot \boldsymbol{\pi}^{\mathrm{CR}} \mathbf{v} = 0$ by Gauss' theorem. Furthermore, there are the well-known stability and approximation properties

$$\|\boldsymbol{\pi}^{\mathrm{CR}} \mathbf{v}\|_{1,h} \leqslant \|\nabla \mathbf{v}\|_0 \quad \text{for all } v \in V, \tag{8}$$

$$\|\mathbf{v} - \boldsymbol{\pi}^{\mathrm{CR}} \mathbf{v}\| \leqslant Ch \|\mathbf{v} - \boldsymbol{\pi}^{\mathrm{CR}} \mathbf{v}\|_{1,h} \quad \text{for all } v \in V, \tag{9}$$

$$\|\mathbf{v} - \boldsymbol{\pi}^{\mathrm{CR}} \mathbf{v}\|_{1,h} \leqslant Ch |\mathbf{v}|_2 \quad \text{for all } v \in V \cap H^2(\Omega)^d, \tag{10}$$

$$\|\mathbf{v} - \boldsymbol{\pi}^{\mathrm{RT}} \mathbf{v}\|_0 \leqslant Ch \|\mathbf{v}\|_{1,h} \quad \text{for all } v \in V \cup \mathrm{CR}(\mathcal{T}), \tag{11}$$

$$\|\mathbf{v} - \boldsymbol{\pi}^{\mathrm{BDM}} \mathbf{v}\|_0 \leqslant Ch \|\mathbf{v}\|_{1,h} \quad \text{for all } v \in V \cup \mathrm{CR}(\mathcal{T}), \tag{12}$$

$$\|\mathbf{v} - \boldsymbol{\pi}^{\mathrm{BDM}} \mathbf{v}\|_0 \leqslant Ch^2 |\mathbf{v}|_2 \quad \text{for all } v \in H^2(\Omega)^d, \tag{13}$$

where the generic constants C depend only on the shape of the simplices in the triangulation $\mathcal{T}$ but not on their size [BF91, AD99, CGR12].

Remark 2. *Note, that the proofs of the estimates (11) and (12) are extendable to functions $\mathbf{v} \in \mathrm{CR}(\mathcal{T})$. For the proof of (12), let Π^{BDM} denote the element-wise projector onto $\mathrm{BDM}(\mathcal{T})$, and $\boldsymbol{\pi}^{\mathrm{BDM}}$ as above. A triangle inequality shows*

$$\|\mathbf{v} - \boldsymbol{\pi}^{\mathrm{BDM}} \mathbf{v}\|_{0,T} \leqslant \|\mathbf{v} - \Pi^{BDM} \mathbf{v}\|_{0,T} + \|\Pi^{BDM} \mathbf{v} - \boldsymbol{\pi}^{\mathrm{BDM}} \mathbf{v}\|_{0,T}$$

and, since Π^{BDM} preserves constants (even linear polynomials) and is bounded on $H^1(T)$, the first term is bounded by $h\|\nabla \mathbf{v}\|_{0,T}$. The second term is a vector-valued linear polynomial on T. By a scaling argument we get

$$\|\Pi^{BDM} \mathbf{v} - \boldsymbol{\pi}^{\mathrm{BDM}} \mathbf{v}\|_{0,T} \leqslant Ch^{1/2} \|\nu \cdot (\Pi^{BDM} \mathbf{v} - \boldsymbol{\pi}^{\mathrm{BDM}} \mathbf{v})\|_{0,\partial T}$$

Since $\left|\nu \cdot (\Pi^{BDM} \mathbf{v} - \boldsymbol{\pi}^{\mathrm{BDM}} \mathbf{v})|_F\right| = \left|\nu \cdot [\pi_{L_2(F)} \mathbf{v}]_F / 2\right|$ for each facet $F \subset \partial T$ with the $L_2(F)$-orthogonal projector $\pi_{L_2(F)}$ onto $P^1(F)$, we observe

$$\|\Pi^{BDM} \mathbf{v} - \pi^{BDM} \mathbf{v}\|_{0,T} \leqslant Ch^{1/2} \|[\mathbf{v}]\|_{0,\partial T}.$$

For $\mathbf{v} \in V \cup CR(\mathcal{T})$ and the face patch $\omega_F := \bigcup_{T \in \mathcal{T}, F \subset \partial T} T$, the last term is bounded by

$$\|[\mathbf{v}]\|_{L_2(F)} \leqslant Ch^{1/2} \|\nabla_h v\|_{0,\omega_F}.$$

2.4. **The finite element scheme with and without divergence-free reconstruction.** The discrete weak formulation of the model problem employs the multilinear forms

$$\begin{aligned}
a_h : \mathrm{CR}(\mathcal{T}) \times \mathrm{CR}(\mathcal{T}) \to \mathbb{R}, \qquad & a_h(\mathbf{u_h}, \mathbf{v}) := \nu \int_\Omega \nabla_h \mathbf{u_h} : \nabla_h \mathbf{v_h} \, dx, \\
b_h : \mathrm{CR}(\mathcal{T}) \times Q \to \mathbb{R}, \qquad & b_h(\mathbf{u_h}, q_h) := -\int_\Omega q_h \nabla_h \cdot \mathbf{u_h} \, dx, \\
c_h : \mathrm{CR}(\mathcal{T}) \times \mathrm{CR}(\mathcal{T}) \times \mathrm{CR}(\mathcal{T}) :\to \mathbb{R}, \qquad & c_h(\mathbf{a_h}, \mathbf{u_h}, \mathbf{v_h}) := \int_\Omega ((\mathbf{a_h} \cdot \nabla_h) \, \mathbf{u_h}) \cdot \mathbf{v_h} \, dx, \\
l_h : \mathrm{CR}(\mathcal{T}) \to \mathbb{R}, \qquad & l_h(\mathbf{v_h}) := \int_\Omega \mathbf{f} \cdot \mathbf{v_h} \, dx.
\end{aligned}$$

Given one of the three interpolation operators above $\boldsymbol{\pi}^{\mathrm{div}} \in \{\boldsymbol{\pi}^{\mathrm{CR}}, \boldsymbol{\pi}^{\mathrm{RT}}, \boldsymbol{\pi}^{\mathrm{BDM}}\}$, the discrete Navier-Stokes problem seeks $(\mathbf{u_h}, p_h) \in \mathrm{CR}(\mathcal{T}) \times Q(\mathcal{T})$ such that

$$\begin{aligned}
a_h(\mathbf{u_h}, \mathbf{v_h}) + \gamma \, c_h(\boldsymbol{\pi}^{\mathrm{div}} \mathbf{u_h}, \mathbf{u_h}, \boldsymbol{\pi}^{\mathrm{div}} \mathbf{v_h}) + b_h(\mathbf{v}, p_h) &= l_h(\boldsymbol{\pi}^{\mathrm{div}} \mathbf{v_h}), \\
b_h(\mathbf{u_h}, q_h) &= 0 \qquad \text{for all } (\mathbf{v_h}, q_h) \in \mathrm{CR}(\mathcal{T}) \times Q(\mathcal{T}).
\end{aligned} \tag{14}$$

The choice $\boldsymbol{\pi}^{\mathrm{div}} = \boldsymbol{\pi}^{\mathrm{CR}}$ leads to the classical Crouzeix-Raviart nonconforming finite element method in the spirit of [CR73], while $\boldsymbol{\pi}^{\mathrm{div}} = \boldsymbol{\pi}^{\mathrm{RT}}$ or $\boldsymbol{\pi}^{\mathrm{div}} = \boldsymbol{\pi}^{\mathrm{BDM}}$ constitute a variational crime that maps discretely divergence-free test functions to divergence-free functions in $H(\mathrm{div}, \Omega)$. The benefits of these divergence-free reconstructions are discussed below.

Remark 3. *The use of $\boldsymbol{\pi}^{\mathrm{div}} \mathbf{v}_h$ in the trilinear form c_h in (14) is needed for stability reasons, because also the nonlinear term $(\mathbf{u} \cdot \nabla)\mathbf{u}$ may have a large irrotational part in the sense of the Helmholtz decomposition* [Lin09].

Like the continuous incompressible Stokes and Navier-Stokes equations, also the discretization (14) can be formulated as an elliptic problem [Tem91, GR86] within the space of discretely divergence-free functions

$$V_{0,h} := \{\mathbf{v}_h \in \mathrm{CR}(\mathcal{T}) : b(\mathbf{v}_h, q_h) = 0 \text{ for all } q_h \in Q(\mathcal{T})\}. \tag{15}$$

Then, $\mathbf{u_h} \in V_{0,h}$ is uniquely defined by

$$a_h(\mathbf{u_h}, \mathbf{v}_h) + \gamma\, c_h(\boldsymbol{\pi}^{\mathrm{div}}\, \mathbf{u_h}, \mathbf{u_h}, \boldsymbol{\pi}^{\mathrm{div}}\, \mathbf{v}_h) = l_h(\boldsymbol{\pi}^{\mathrm{div}}\, \mathbf{v}_h) \quad \text{for all } \mathbf{v}_h \in V_{0,h}. \tag{16}$$

Remark 4. *The pair $\mathrm{CR}(\mathcal{T}) \times Q(\mathcal{T})$ satisfies the discrete inf-sup condition*

$$0 < \beta := \inf_{q_h \in Q(\mathcal{T})\setminus\{0\}} \sup_{\mathbf{v}_h \in \mathrm{CR}(\mathcal{T})\setminus\{0\}} \frac{\int_\Omega q_h \nabla_h \cdot \mathbf{v}_h \, dx}{\|\mathbf{v}_h\|_{1,h} \|q\|_0}. \tag{17}$$

The inf-sup constant β for the Crouzeix-Raviart element is independent of the mesh and of the reconstruction $\boldsymbol{\pi}^{\mathrm{div}}$.

3. A Priori Error Estimates

This section presents a priori finite element error estimates for the modified Crouzeix-Raviart discretization of the incompressible Stokes equations (14). The analysis is based on the estimates of the consistency error in [AD99], which apply the Raviart-Thomas interpolation to the best advantage and avoid the use of a trace inequality. However, some slight changes due to the divergence-conforming reconstruction deliver fundamentally improved results, since the scheme (14) allows for an error estimate of the discrete velocity that is independent of the pressure.

Lemma 1. *For $\boldsymbol{\pi}^{\mathrm{div}} = \boldsymbol{\pi}^{\mathrm{RT}}$ or $\boldsymbol{\pi}^{\mathrm{div}} = \boldsymbol{\pi}^{\mathrm{BDM}}$, it holds*

$$\left| \int_\Omega \nabla_h \mathbf{v} : \nabla_h \mathbf{w} + \Delta \mathbf{v} \cdot \boldsymbol{\pi}^{\mathrm{div}}\, \mathbf{w} \, dx \right| \leqslant Ch|\mathbf{v}|_2 \|\mathbf{w}\|_{1,h} \quad \textit{for all } \mathbf{v} \in V \cap H^2(\Omega)^d, \mathbf{w} \in V \cup \mathrm{CR}(\mathcal{T}).$$

Proof. The proof can be found in [Lin14] for $\boldsymbol{\pi}^{\mathrm{div}} = \boldsymbol{\pi}^{\mathrm{RT}}$ and is the same for $\boldsymbol{\pi}^{\mathrm{div}} = \boldsymbol{\pi}^{\mathrm{BDM}}$. For the sake of completeness and convenience, it is repeated here in a shortened form.

Let $\boldsymbol{\Pi}^{\mathrm{RT}}$ denote the rowwise Raviart-Thomas interpolator and Π_0 the L^2 projection onto $P_0(\mathcal{T})^d$. Since the normal fluxes $(\boldsymbol{\Pi}^{\mathrm{RT}} \nabla \mathbf{v}) \cdot \mathbf{n}_F$ are continuous for all $F \in \mathcal{F}$ and constant on the boundary faces $F \in \mathcal{F}(\partial\Omega)$ and $\mathbf{w}$ is zero at least at the centers of any $F \in \mathcal{F}(\partial\Omega)$, it holds

$$\sum_{T \in \mathcal{T}} \int_{\partial T} \boldsymbol{\Pi}^{\mathrm{RT}} \nabla \mathbf{v} \cdot \mathbf{n}\, w \, ds = 0.$$

An elementwise integration by parts and the commutation property $\nabla \cdot (\boldsymbol{\Pi}^{\mathrm{RT}} \nabla \mathbf{v}) = \Pi_0(\Delta \mathbf{v})$, show

$$\int_\Omega \boldsymbol{\Pi}^{\mathrm{RT}} \nabla \mathbf{v} \cdot \nabla_h \mathbf{w} + \Pi_0(\Delta \mathbf{v}) \cdot \mathbf{w} \, dx = 0.$$

This and elementary calculations reveal

$$\begin{aligned}&\int_\Omega \nabla_h \mathbf{v} : \nabla_h \mathbf{w}_h + \Delta \mathbf{v} \cdot \boldsymbol{\pi}^{\mathrm{div}} \mathbf{w}_h \, dx \\ &= \int_\Omega \left(\nabla_h \mathbf{v} - \boldsymbol{\Pi}^{\mathrm{RT}} \nabla \mathbf{v}\right) : \nabla_h \mathbf{w}_h \, dx + \int_\Omega (\Delta \mathbf{v} - \Pi_0(\Delta \mathbf{v})) \cdot \mathbf{w} \, dx + \int_\Omega \Delta \mathbf{v} \cdot \left(\boldsymbol{\pi}^{\mathrm{div}} \mathbf{w} - \mathbf{w}\right) dx.\end{aligned}$$

The first integral is estimated with a Cauchy-Schwarz inequality and the rowwise version of (11), while the third integral is estimated by a Cauchy-Schwarz inequality and (11) (for $\boldsymbol{\pi}^{\mathrm{div}} = \boldsymbol{\pi}^{\mathrm{RT}}$) or (12) (for $\boldsymbol{\pi}^{\mathrm{div}} = \boldsymbol{\pi}^{\mathrm{BDM}}$). The second integral is estimated with the L^2 orthogonality of $\Delta \mathbf{v} - \Pi_0(\Delta \mathbf{v})$ and $\mathbf{w} - \Pi_0 \mathbf{w}$ w.r.t. $P_0(\mathcal{T})^d$ by

$$\int_\Omega (\Delta \mathbf{v} - \Pi_0(\Delta \mathbf{v})) \cdot \mathbf{w} \, dx = \int_\Omega (\Delta \mathbf{v} - \Pi_0(\Delta \mathbf{v})) \cdot (\mathbf{w} - \Pi_0 \mathbf{w}) \, dx \leqslant \|\Delta \mathbf{v}\|_0 \|\mathbf{w} - \Pi_0 \mathbf{w}\|_0.$$

An elementwise Poincaré inequality concludes the proof. □

The estimate of the consistency error is a corollary to Lemma 1.

Lemma 2 (Consistency error estimate)**.** *Given the solution $(\mathbf{u}, p) \in H^2(\Omega)^d \times H^1(\Omega)$ of the continuous Stokes equations (4) and $\boldsymbol{\pi}^{\mathrm{div}} = \boldsymbol{\pi}^{\mathrm{RT}}$ or $\boldsymbol{\pi}^{\mathrm{div}} = \boldsymbol{\pi}^{\mathrm{BDM}}$, it holds*

$$\frac{1}{\nu} \sup_{\mathbf{w}_h \in V_0 + V_{0,h}} \frac{\left| a_h(\mathbf{u}, \mathbf{w}_h) - l_h(\boldsymbol{\pi}^{\mathrm{div}} \mathbf{w}_h) \right|}{\|\mathbf{w}_h\|_{1,h}} \leqslant Ch|\mathbf{u}|_2$$

holds.

Proof. For all $\mathbf{0} \neq \mathbf{w}_h \in V_0 + V_{0,h}$, (4) and $\int_\omega \nabla p : \boldsymbol{\pi}^{\mathrm{div}} \mathbf{w} \, dx = 0$ show

$$\begin{aligned}\frac{1}{\nu} \left| a_h(\mathbf{u}, \mathbf{w}_h) - l_h(\boldsymbol{\pi}^{\mathrm{div}} \mathbf{w}_h) \right| &= \frac{1}{\nu} \left| \int_\Omega \nu \nabla_h \mathbf{u} : \nabla_h \mathbf{w}_h - \mathbf{f} \cdot \boldsymbol{\pi}^{\mathrm{div}} \mathbf{w}_h \, dx \right| \\ &= \frac{1}{\nu} \left| \int_\Omega \nu \nabla_h \mathbf{u} : \nabla_h \mathbf{w}_h + (\nu \Delta \mathbf{u} - \nabla p) \cdot \boldsymbol{\pi}^{\mathrm{div}} \mathbf{w}_h \, dx \right| \\ &= \left| \int_\Omega \nabla_h \mathbf{u} : \nabla_h \mathbf{w}_h + \Delta \mathbf{u} \cdot \boldsymbol{\pi}^{\mathrm{div}} \mathbf{w}_h \, dx \right|.\end{aligned} \tag{18}$$

Lemma 1 concludes the proof. □

Remark 5. *Note that Lemma 2 does not hold for $\boldsymbol{\pi}^{\mathrm{div}} = \boldsymbol{\pi}^{\mathrm{CR}}$, since in (18) ∇p and $\boldsymbol{\pi}^{\mathrm{CR}} \mathbf{w_h}$ for $w_h \in V_0 + V_{0,h}$ are not orthogonal in the L^2 scalar product.*

The estimate of the consistency error leads to the following a priori estimates.

Theorem 1. *For the solution $(\mathbf{u}, p) \in H^2(\Omega)^d \times H^1(\Omega)$ of the continuous Stokes equations (4) and the discrete solution $(\mathbf{u}_h, p_h)$ of (14) with $\boldsymbol{\pi}^{\mathrm{div}} = \boldsymbol{\pi}^{\mathrm{RT}}$ or $\boldsymbol{\pi}^{\mathrm{div}} = \boldsymbol{\pi}^{\mathrm{BDM}}$, it holds*

$$\begin{aligned} &i) \qquad \|\mathbf{u} - \mathbf{u}_h\|_{1,h} \leqslant Ch \, |\mathbf{u}|_2 \,, \\ &ii) \qquad \|p - p_h\|_0 \leqslant C \, h \, (\nu \, |\mathbf{u}|_2 + |p|_1) \,. \end{aligned}$$

Proof of i). Formulation (16) and $\mathbf{w}_h := \mathbf{u}_h - \mathbf{v}_h$ for an arbitrary $\mathbf{v}_h \in V_{0,h}$ yield

$$\begin{aligned}\nu \|\mathbf{w}_h\|_{1,h}^2 &= a_h(\mathbf{w}_h, \mathbf{w}_h) \\ &= a_h(\mathbf{u}_h - \mathbf{v}_h, \mathbf{w}_h) \\ &= a_h(\mathbf{u}_h - \mathbf{v}_h, \mathbf{w}_h) + a_h(\mathbf{u}_h, \mathbf{w}_h) - a(\mathbf{u}_h, \mathbf{w}_h) \\ &= a_h(\mathbf{u}_h - \mathbf{v}_h, \mathbf{w}_h) + l_h(\boldsymbol{\pi}^{\mathrm{div}} \mathbf{w}_h) - a_h(\mathbf{u}_h, \mathbf{w}_h) \\ &\leqslant \nu \|\mathbf{u}_h - \mathbf{v}_h\|_{1,h} \|\mathbf{w}_h\|_{1,h} + \left| a_h(\mathbf{u}_h, \mathbf{w}_h) - l_h(\boldsymbol{\pi}^{\mathrm{div}} \mathbf{w}_h) \right|.\end{aligned}$$

The triangle inequality for $\|\mathbf{u}-\mathbf{u}_h\|_{1,h} = \|(\mathbf{u}-\mathbf{v}_h)-\mathbf{w}_h\|_{1,h}$ produces Strang's second lemma in the form

$$\|\mathbf{u}-\mathbf{u}_h\|_{1,h} \leqslant 2 \inf_{\mathbf{v}_h\in V_{0,h}} \|\mathbf{u}-\mathbf{v}_h\|_{1,h} + \frac{1}{\nu} \sup_{\mathbf{w}_h\in V_{0,h}} \frac{\left|a_h(\mathbf{u},\mathbf{w}_h) - l_h(\boldsymbol{\pi}^{\mathrm{div}}\,\mathbf{w}_h)\right|}{\|\mathbf{w}_h\|_{1,h}}.$$

The first error term can be bounded with (10) by

$$\inf_{\mathbf{v}_h\in V_{0,h}} \|\mathbf{u}-\mathbf{v}_h\|_{1,h} \leqslant \|\mathbf{u}-\boldsymbol{\pi}^{\mathrm{CR}}\,\mathbf{u}\|_{1,h} \leqslant Ch|\mathbf{u}|_2.$$

Note, that C is independent of the discrete inf-sup-constant β from (17), since $\boldsymbol{\pi}^{\mathrm{CR}}\,\mathbf{u} \in V_{0,h}$. The second error term is estimated with Lemma 2. □

Proof of ii). For the pressure estimate, the Pythagoras theorem shows

$$\|p-p_h\|_0^2 = \|p-\pi_0 p\|_0^2 + \|\pi_0 p - p_h\|_0^2.$$

Obviously, the first term is bounded by

$$\|p-\pi_0 p\|_0 \leqslant Ch\,|p|_1\,.$$

Due to the discrete inf-sup stability (17), we can estimate the second term by

$$\|\pi_0 p - p_h\|_0 \leqslant \frac{1}{\beta} \sup_{\mathbf{v}_h\in \mathrm{CR}(\mathcal{T})} \frac{b_h(\mathbf{v}_h, \pi_0 p - p - h)}{\|\mathbf{v}_h\|_{1,h}}.$$

The term in the numerator of this expression consists of the two parts

$$b_h(\mathbf{v}_h, \pi_0 p - p_h) = b_h(\mathbf{v}_h, \pi_0 p - p_h) + b_h(\mathbf{v}_h, p - p_h).$$

The first term can be estimated by

$$|b_h(\mathbf{v}_h, \pi_0 p - p_h)| \leqslant \sqrt{d}\,\|\mathbf{v}_h\|_{1,h}\|p_h - \pi_0 p\|_0 \leqslant Ch\,|p|_1 \cdot \|\mathbf{v}_h\|_{1,h}.$$

For the second term, one computes

$$\begin{aligned} b_h(\mathbf{v}_h, p-p_h) &= b_h(\mathbf{v}_h, p) + a_h(\mathbf{u}_h, \mathbf{v}_h) - l_h(\boldsymbol{\pi}^{\mathrm{div}}\,\mathbf{v}_h) \\ &= a_h(\mathbf{u}_h - \mathbf{u}, \mathbf{v}_h) + \int_\Omega \left\{ \nu \nabla_h \mathbf{u} : \nabla_h \mathbf{v}_h - p \nabla_h \cdot \mathbf{v}_h - \mathbf{f} \cdot \boldsymbol{\pi}^{\mathrm{div}}\,\mathbf{v}_h \right\} dx \\ &= a_h(\mathbf{u}_h - \mathbf{u}, \mathbf{v}_h) + \int_\Omega \nu \left\{ \nabla_h \mathbf{u} : \nabla \mathbf{v}_h + \Delta \mathbf{u} \cdot \boldsymbol{\pi}^{\mathrm{div}}\,\mathbf{v}_h \right\} dx, \end{aligned}$$

since

$$\int_\Omega \left\{ -p\nabla_h \cdot \mathbf{v}_h - \nabla p \cdot \left(\boldsymbol{\pi}^{\mathrm{div}}\,\mathbf{v}_h \right) \right\} dx = \int_\Omega \left\{ -p\nabla_h \cdot \mathbf{v}_h + p\nabla \cdot \left(\boldsymbol{\pi}^{\mathrm{div}}\,\mathbf{v}_h \right) \right\} dx = 0.$$

Eventually, this results in the estimate

$$b_h(\mathbf{v}, p-p_h) \leqslant C\nu h\,|\mathbf{u}|_2\,\|\mathbf{v}_h\|_{1,h}.$$

The combination of all estimates leads to

$$\|p-p_h\|_0 \leqslant C \left\{ \frac{1}{\beta}\nu\,|\mathbf{u}|_2 + \left(1 + \frac{1}{\beta}\right) |p|_1 \right\} h.$$

□

4. Optimal L^2-convergence

For convex domains, the new discretization scheme (14) with $\boldsymbol{\pi}^{\mathrm{div}} = \boldsymbol{\pi}^{\mathrm{BDM}}$ allows an additional optimal L^2 error estimate for the discrete velocity, see Theorem 2 below.

Lemma 3. *Given a right-hand side $\mathbf{g} \in L^2(\Omega)^d$, let $\mathbf{u}_g \in V_0$ denote the solution of*

$$a(\mathbf{u}_g, \mathbf{v}) = (\mathbf{g}, \mathbf{v}) \quad \text{for all } \mathbf{v} \in V_0,$$

and let $\mathbf{u}_{g,h} \in V_{0,h}$ denote the solution of

$$a_h(\mathbf{u}_{g,h}, \mathbf{v}_h) = (\mathbf{g}, \boldsymbol{\pi}^{\mathrm{div}}\, \mathbf{v}_h) \quad \text{for all } \mathbf{v}_h \in V_{0,h}$$

Then, for the solutions $\mathbf{u}$ from (4) and $\mathbf{u}_h$ from (14), it holds

$$\begin{aligned}\|\mathbf{u} - \mathbf{u}_h\|_0 \leqslant \sup_{\mathbf{g}\in L^2(\Omega)^d, \|\mathbf{g}\|_0=1} \Big\{ & \nu \|\mathbf{u} - \mathbf{u}_h\|_{1,h} \|\mathbf{u}_g - \mathbf{u}_{g,h}\|_{1,h} \\ & + \Big| a_h(\mathbf{u} - \mathbf{u}_h, \mathbf{u}_g) - \Big(\mathbf{g}, \boldsymbol{\pi}^{\mathrm{div}}\, (\mathbf{u} - \mathbf{u}_h)\Big) \Big| \\ & + \Big| a_h(\mathbf{u}, \mathbf{u}_g - \mathbf{u}_{g,h}) - \Big(\mathbf{f}, \boldsymbol{\pi}^{\mathrm{div}}\, (\mathbf{u}_g - \mathbf{u}_{g,h})\Big) \Big| \\ & + \Big| \Big(\mathbf{g}, (\mathbf{u} - \mathbf{u}_h) - \boldsymbol{\pi}^{\mathrm{div}}\, (\mathbf{u} - \mathbf{u}_h)\Big) \Big| \\ & + \Big| \Big(\mathbf{f}, \mathbf{u}_g - \boldsymbol{\pi}^{\mathrm{div}}\, \mathbf{u}_g\Big) \Big| \Big\}.\end{aligned}$$

Proof. The proof is based on the duality argument

$$\|\mathbf{u} - \mathbf{u}_h\|_0 = \sup_{\mathbf{g}\in L^2(\Omega)^d} (\mathbf{g}, \mathbf{u} - \mathbf{u}_h) / \|\mathbf{g}\|_0.$$

Elementary algebra yields

$$\begin{aligned}(\mathbf{g}, \mathbf{u} - \mathbf{u}_h) &= a_h(\mathbf{u}_h, \mathbf{u}_{g,h}) - a_h(\mathbf{u}, \mathbf{u}_g) + (\mathbf{g}, \mathbf{u} - \mathbf{u}_h) + \Big(\mathbf{f}, \mathbf{u}_g - \boldsymbol{\pi}^{\mathrm{div}}\, \mathbf{u}_{g,h}\Big) \\ &= -a_h(\mathbf{u} - \mathbf{u}_h, \mathbf{u}_{g,h}) - a_h(\mathbf{u}, \mathbf{u}_g - \mathbf{u}_{g,h}) \\ &\quad + (\mathbf{g}, \mathbf{u} - \mathbf{u}_h) + \Big(\mathbf{f}, \mathbf{u}_g - \boldsymbol{\pi}^{\mathrm{div}}\, \mathbf{u}_{g,h}\Big) \\ &= a_h(\mathbf{u} - \mathbf{u}_h, \mathbf{u}_g - \mathbf{u}_{g,h}) \\ &\quad - a_h(\mathbf{u} - \mathbf{u}_h, \mathbf{u}_g) + \Big(\mathbf{g}, \boldsymbol{\pi}^{\mathrm{div}}\, (\mathbf{u} - \mathbf{u}_h)\Big) \\ &\quad - a_h(\mathbf{u}, \mathbf{u}_g - \mathbf{u}_{g,h}) + \Big(\mathbf{f}, \boldsymbol{\pi}^{\mathrm{div}}\, (\mathbf{u}_g - \mathbf{u}_{g,h})\Big) \\ &\quad + \Big(\mathbf{g}, (\mathbf{u} - \mathbf{u}_h) - \boldsymbol{\pi}^{\mathrm{div}}\, (\mathbf{u} - \mathbf{u}_h)\Big) \\ &\quad + \Big(\mathbf{f}, \mathbf{u}_g - \boldsymbol{\pi}^{\mathrm{div}}\, \mathbf{u}_g\Big).\end{aligned}$$

Triangle and Cauchy-Schwarz inequalities conclude the proof. □

Theorem 2. *For a convex domain Ω the exact solution $(\mathbf{u}, p) \in H^2(\Omega)^d \times H^1(\Omega)$ of the continuous Stokes equations (4) and the discrete solution $(\mathbf{u}_h, p_h)$ of (14) for $\boldsymbol{\pi}^{\mathrm{div}} = \boldsymbol{\pi}^{\mathrm{BDM}}$ satisfy an optimal L^2 error estimate for the discrete velocity, i.e.,*

$$\|\mathbf{u} - \mathbf{u}_h\|_0 \leqslant C\, h^2\, |\mathbf{u}|_2\,.$$

Proof. Since Ω is convex, classical regularity results for the incompressible Stokes equations imply $\mathbf{u}_g \in H^2(\Omega)^d$ and the a priori estimate

$$\nu \left(|\mathbf{u}_g|_2 + \|\nabla \mathbf{u}_g\|_0\right) \leqslant C \|\mathbf{g}\|_0 \quad \text{for all } \mathbf{g} \in L^2(\Omega)^d. \tag{19}$$

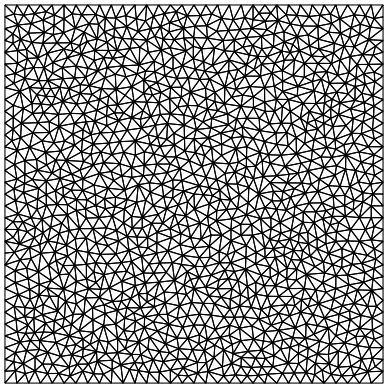

FIGURE 1. Initial mesh for the numerical examples

The rest of the proof uses this estimate to bound the five terms in the estimate of Lemma 3. For the first term, Theorem 1 and (19) show

$$\nu\|\mathbf{u}-\mathbf{u}_h\|_{1,h}\|\mathbf{u}_g-\mathbf{u}_{g,h}\|_{1,h} \leqslant \nu\left(Ch\,|\mathbf{u}|_2\right)\cdot\left(Ch\,|\mathbf{u}_g|_2\right) \leqslant Ch^2\,|\mathbf{u}|_2\,\|\mathbf{g}\|_0.$$

The second term is estimated by the consistency error from Lemma 2, Theorem 1 and (19),

$$\left|a_h(\mathbf{u}-\mathbf{u}_h,\mathbf{u}_g)-\left(\mathbf{g},\boldsymbol{\pi}^{\mathrm{BDM}}(\mathbf{u}-\mathbf{u}_h)\right)\right| \leqslant \nu Ch\,|\mathbf{u}_g|_2\,\|\mathbf{u}-\mathbf{u}_h\|_{1,h} \leqslant Ch^2\,|\mathbf{u}|_2\,\|\mathbf{g}\|_0.$$

Similar arguments yield

$$\begin{aligned}\left|a_h(\mathbf{u},\mathbf{u}_g-\mathbf{u}_{g,h})-\left(\mathbf{f},\boldsymbol{\pi}^{\mathrm{BDM}}(\mathbf{u}_g-\mathbf{u}_{g,h})\right)\right| &\leqslant \nu Ch\,|\mathbf{u}|_2\,\|\mathbf{u}_g-\mathbf{u}_{g,h}\|_{1,h}\\ &\leqslant \nu Ch^2\,|\mathbf{u}|_2\,|\mathbf{u}_g|_2\\ &\leqslant Ch^2\,|\mathbf{u}|_2\,\|\mathbf{g}\|_0.\end{aligned}$$

Theorem 1 bounds the fourth term by

$$\left|\left(\mathbf{g},(\mathbf{u}-\mathbf{u}_h)-\boldsymbol{\pi}^{\mathrm{BDM}}(\mathbf{u}-\mathbf{u}_h)\right)\right| \leqslant Ch\|\mathbf{u}-\mathbf{u}_h\|_{1,h}\|\mathbf{g}\|_0 \leqslant Ch^2\,|\mathbf{u}|_2\,\|\mathbf{g}\|_0.$$

For the last term, $-\nu\Delta\mathbf{u}+\nabla p=\mathbf{f}$ and (13) show

$$\begin{aligned}\left|\left(\mathbf{f},\mathbf{u}_g-\boldsymbol{\pi}^{\mathrm{BDM}}\mathbf{u}_g\right)\right| = \left|\left(-\nu\Delta\mathbf{u},\mathbf{u}_g-\boldsymbol{\pi}^{\mathrm{BDM}}\mathbf{u}_g\right)\right| &\leqslant C\nu|\mathbf{u}|_2\|\mathbf{u}_g-\boldsymbol{\pi}^{\mathrm{BDM}}\mathbf{u}_g\|_0\\ &\leqslant Ch^2\nu|\mathbf{u}|_2|\mathbf{u}_g|_2\\ &\leqslant Ch^2|\mathbf{u}|_2\|\mathbf{g}\|_0.\end{aligned}$$

The sum of all previous estimates concludes the proof. □

5. Numerical Results

This section reports on some numerical results. All examples are computed on a series of unstructured triangulations of the unit square. The initial mesh is depicted in Figure 1.

5.1. **First Example.** The first benchmark example concerns the Stokes problem for the stream function $\xi = x^2(1-x)^2y^2(1-y)^2$ with $\mathbf{u}=\mathrm{rot}\,\xi \in P_7(\Omega)^2\cap V$ and $p=x^3+y^3-1/2$ on the unit square $\Omega=(0,1)^2$. For given viscosity ν, the volume force equals $\mathbf{f}:=-\nu\Delta\mathbf{u}+\nabla p$. Figure 2 displays the exact velocity $\mathbf{u}$ and the pressure p.

Tables 1-3 compare the results of the three methods under consideration for $\nu=10^{-2}$. While the error in the pressure is only slightly smaller, the H^1 error in the velocity is more than two magnitudes smaller for the methods with a divergence-free reconstruction. This is exactly the influence of the $1/\nu\,|p|_1$ contribution in the classical velocity error estimate (2). However, in this example there seems to be no additional benefit when $\boldsymbol{\pi}^{\mathrm{BDM}}$ is employed

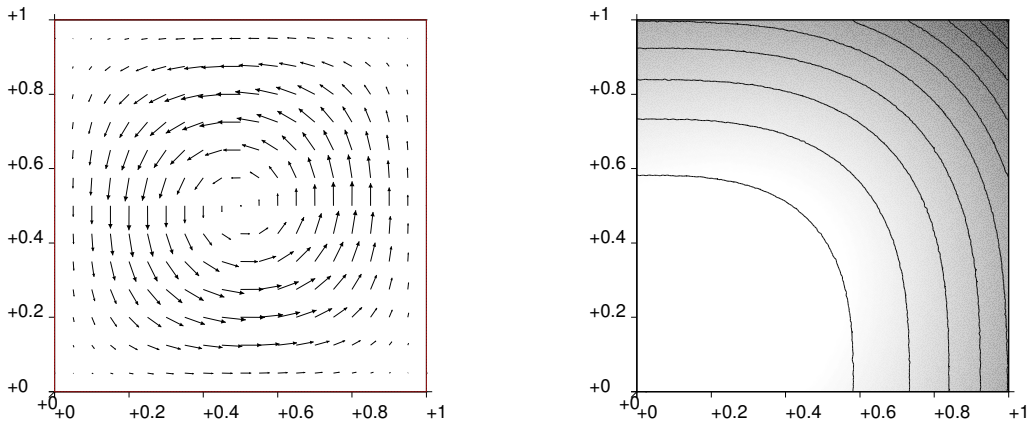

FIGURE 2. Vector plot of $\mathbf{u}$ and contour plot of p from the benchmark problem of Section 5.1.

ndof	$\|\mathbf{u}-\mathbf{u}_h\|_0 \quad (\boldsymbol{\pi}^{\mathrm{CR}})$	$\|\mathbf{u}-\mathbf{u}_h\|_0 \quad (\boldsymbol{\pi}^{\mathrm{RT}})$	$\|\mathbf{u}-\mathbf{u}_h\|_0 \quad (\boldsymbol{\pi}^{\mathrm{BDM}})$
10176	1.462715e-02	5.738088e-05	6.475907e-05
40488	3.714616e-03	1.468924e-05	1.651350e-05
162152	9.311043e-04	3.655164e-06	4.117682e-06
646376	2.346116e-04	9.201573e-07	1.036546e-06
2585272	5.889322e-05	2.299916e-07	2.589664e-07

TABLE 1. L^2-error for the velocity in the benchmark problem of Section 5.1.

ndof	$\|\mathbf{u}-\mathbf{u}_h\|_{1,h} \quad (\boldsymbol{\pi}^{\mathrm{CR}})$	$\|\mathbf{u}-\mathbf{u}_h\|_{1,h} \quad (\boldsymbol{\pi}^{\mathrm{RT}})$	$\|\mathbf{u}-\mathbf{u}_h\|_{1,h} \quad (\boldsymbol{\pi}^{\mathrm{BDM}})$
10176	1.333391	6.189144e-03	6.184352e-03
40488	6.688239e-01	3.115982e-03	3.115428e-03
162152	3.349285e-01	1.556097e-03	1.556023e-03
646376	1.682897e-01	7.801799e-04	7.801701e-04
2585272	8.432380e-02	3.899851e-04	3.899841e-04

TABLE 2. Energy error for the velocity in the benchmark problem of Section 5.1.

ndof	$\|p-p_h\|_0 \quad (\boldsymbol{\pi}^{\mathrm{CR}})$	$\|p-p_h\|_0 \quad (\boldsymbol{\pi}^{\mathrm{RT}})$	$\|p-p_h\|_0 \quad (\boldsymbol{\pi}^{\mathrm{BDM}})$
10176	1.293413e-02	1.270086e-02	1.270086e-02
40488	6.371610e-03	6.297825e-03	6.297825e-03
162152	3.174234e-03	3.147287e-03	3.147287e-03
646376	1.590767e-03	1.579164e-03	1.579164e-03
2585272	7.960010e-04	7.904408e-04	7.904408e-04

TABLE 3. L^2-error for the pressure in the benchmark problem of Section 5.1.

instead of $\boldsymbol{\pi}^{\mathrm{RT}}$. Moreover, the convergence speed of the L^2-error in the velocity is optimal also for $\boldsymbol{\pi}^{\mathrm{RT}}$.

5.2. **Second Example.** The second example concerns the Navier-Stokes problem with the exact solution from the first example for $\nu = 10^{-2}$ and $\mathbf{f} := -\nu\Delta\mathbf{u} + \nabla p + (\mathbf{u}\cdot\nabla)\mathbf{u}$.

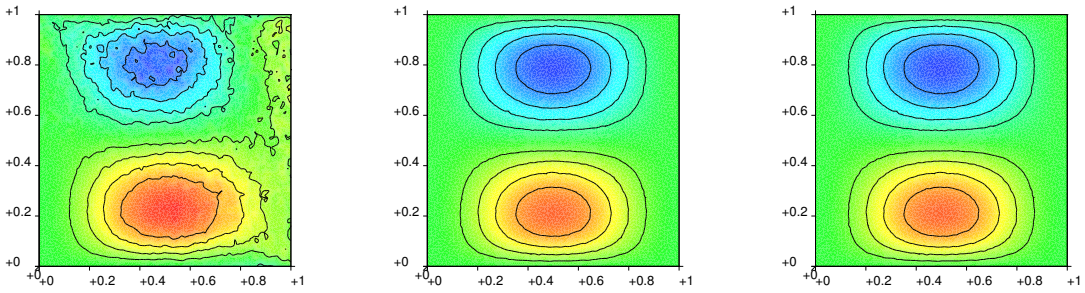

FIGURE 3. Isolines for the first component of the discrete solution u of Section 5.2 for $\boldsymbol{\pi}^{\mathrm{div}} = \boldsymbol{\pi}^{\mathrm{CR}}$ (left), $\boldsymbol{\pi}^{\mathrm{div}} = \boldsymbol{\pi}^{\mathrm{RT}}$ (middle) and $\boldsymbol{\pi}^{\mathrm{div}} = \boldsymbol{\pi}^{\mathrm{BDM}}$ (right).

Figure 3 displays the isolines $\{x \in \Omega : u_1(x) = \pm 0.005n\}_{n=1,\dots,4}$ of the first component of the discrete velocity on the second refinement level. The pollutive effect of the pressure-dependence of the velocity discretization in the unreconstructed method ($\boldsymbol{\pi}^{\mathrm{div}} = \boldsymbol{\pi}^{\mathrm{CR}}$) is clearly visible in the left subfigure. The visible oscillations must be related to the poor momentum balance and not to dominant convection.

Tables 4-6 compare the results of the three methods. The observations appear similar to the ones in the first example. The methods with a divergence-free reconstruction are clearly superior to the original Crouzeix-Raviart discretization, but there is no additional gain from the utilization of $\boldsymbol{\pi}^{\mathrm{BDM}}$ instead of $\boldsymbol{\pi}^{\mathrm{RT}}$ also in this example.

ndof	$\|\mathbf{u}-\mathbf{u}_h\|_0 \quad (\boldsymbol{\pi}^{\mathrm{CR}})$	$\|\mathbf{u}-\mathbf{u}_h\|_0 \quad (\boldsymbol{\pi}^{\mathrm{RT}})$	$\|\mathbf{u}-\mathbf{u}_h\|_0 \quad (\boldsymbol{\pi}^{\mathrm{BDM}})$
10176	1.461456e-02	5.627152e-05	6.379470e-05
40488	3.714998e-03	1.442375e-05	1.627764e-05
162152	9.313632e-04	3.588727e-06	4.059383e-06
646376	2.346806e-04	9.033673e-07	1.021663e-06
2585272	5.890854e-05	2.257938e-07	2.552337e-07

TABLE 4. L^2-error for the velocity in the benchmark problem of Section 5.2.

ndof	$\|\mathbf{u}-\mathbf{u}_h\|_{1,h} \quad (\boldsymbol{\pi}^{\mathrm{CR}})$	$\|\mathbf{u}-\mathbf{u}_h\|_{1,h} \quad (\boldsymbol{\pi}^{\mathrm{RT}})$	$\|\mathbf{u}-\mathbf{u}_h\|_{1,h} \quad (\boldsymbol{\pi}^{\mathrm{BDM}})$
10176	1.333839	6.188967e-03	6.184106e-03
40488	6.688321e-01	3.115955e-03	3.115408e-03
162152	3.349292e-01	1.556094e-03	1.556020e-03
646376	1.682898e-01	7.801796e-04	7.801695e-04
2585272	8.432380e-02	3.899850e-04	3.899841e-04

TABLE 5. Energy error for the velocity in the benchmark problem of Section 5.2.

ndof	$\|p-p_h\|_0 \quad (\boldsymbol{\pi}^{\mathrm{CR}})$	$\|p-p_h\|_0 \quad (\boldsymbol{\pi}^{\mathrm{RT}})$	$\|p-p_h\|_0 \quad (\boldsymbol{\pi}^{\mathrm{BDM}})$
10176	1.292384e-02	1.269931e-02	1.269931e-02
40488	6.370451e-03	6.297503e-03	6.297503e-03
162152	3.174027e-03	3.147346e-03	3.147346e-03
646376	1.591016e-03	1.579546e-03	1.579546e-03
2585272	7.968145e-04	7.913264e-04	7.913264e-04

TABLE 6. L^2-error for the pressure in the benchmark problem of Section 5.2.

ndof	$\|\mathbf{u}-\mathbf{u}_h\|_0 \quad (\boldsymbol{\pi}^{\mathrm{CR}})$	$\|\mathbf{u}-\mathbf{u}_h\|_0 \quad (\boldsymbol{\pi}^{\mathrm{RT}})$	$\|\mathbf{u}-\mathbf{u}_h\|_0 \quad (\boldsymbol{\pi}^{\mathrm{BDM}})$
10176	0	1.149124e-04	1.428228e-05
40488	0	1.777836e-05	1.835523e-06
162152	0	2.240175e-06	2.202933e-07

TABLE 7. L^2-error for the velocity in the benchmark problem of Section 5.3.

ndof	$\|\mathbf{u}-\mathbf{u}_h\|_{1,h} \quad (\boldsymbol{\pi}^{\mathrm{CR}})$	$\|\mathbf{u}-\mathbf{u}_h\|_{1,h} \quad (\boldsymbol{\pi}^{\mathrm{RT}})$	$\|\mathbf{u}-\mathbf{u}_h\|_{1,h} \quad (\boldsymbol{\pi}^{\mathrm{BDM}})$
10176	0	7.319293e-03	7.146433e-04
40488	0	1.904265e-03	1.433772e-04
162152	0	4.778662e-04	2.428478e-05

TABLE 8. Energy error for the velocity in the benchmark problem of Section 5.3.

ndof	$\|p-p_h\|_0 \quad (\boldsymbol{\pi}^{\mathrm{CR}})$	$\|p-p_h\|_0 \quad (\boldsymbol{\pi}^{\mathrm{RT}})$	$\|p-p_h\|_0 \quad (\boldsymbol{\pi}^{\mathrm{BDM}})$
10176	0	6.968692e-03	1.426464e-03
40488	0	1.661379e-03	2.524422e-04
162152	0	4.130402e-04	4.430947e-05

TABLE 9. L^2-error for the pressure in the benchmark problem of Section 5.3.

5.3. **Third Example.** The third example concerns the Navier-Stokes problem for the affine exact solution $\mathbf{u}(x,y) = (2+3x+5y, 13+17x-3y)$ and $p \equiv 0$ for $\nu = 1$ and $\mathbf{f} = -\Delta\mathbf{u}+(\mathbf{u}\cdot\nabla)\mathbf{u}$.

Tables 7-9 compare the results of the three methods. Note, that $\mathbf{u} \in \mathrm{CR}(\mathcal{T}) \cap \mathrm{BDM}(\mathcal{T})$ but $\mathbf{u} \notin \mathrm{RT}(\mathcal{T})$. While $\mathbf{u}_h \equiv \mathbf{u}$ for $\boldsymbol{\pi}^{\mathrm{div}} = \boldsymbol{\pi}^{\mathrm{CR}}$, the discrete solution cannot equal the exact solution in case $\boldsymbol{\pi}^{\mathrm{div}} = \boldsymbol{\pi}^{\mathrm{RT}}$. However, the BDM interpolation $\boldsymbol{\pi}^{\mathrm{div}} = \boldsymbol{\pi}^{\mathrm{BDM}}$ yields less interpolation errors, which positively affects the overall performance. All errors for $\boldsymbol{\pi}^{\mathrm{div}} = \boldsymbol{\pi}^{\mathrm{BDM}}$ are about one magnitude smaller than the errors for $\boldsymbol{\pi}^{\mathrm{div}} = \boldsymbol{\pi}^{\mathrm{RT}}$. The remaining error for $\boldsymbol{\pi}^{\mathrm{div}} = \boldsymbol{\pi}^{\mathrm{BDM}}$ stems from the nonoptimal interpolation $\boldsymbol{\pi}^{\mathrm{BDM}}\,\mathbf{u} = \boldsymbol{\pi}^{\mathrm{RT}}\,\mathbf{u}$ on the edges $\mathcal{F}(\partial\Omega)$ along the boundary $\partial\Omega$ of the domain.

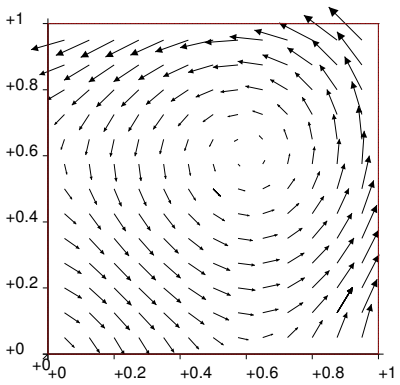

FIGURE 4. Plot of $\mathbf{u}$ from the benchmark problem of Section 5.4 for $s = 2$.

5.4. **Fourth Example.** The last example studies the influence of the regularity of the solution on the L^2-error convergence rate and considers the Stokes problem for $p \equiv 0$ and

$$\mathbf{u}(x,y) = \mathrm{rot}(x^s \log(x) + y^s \log(y))/5 \in H^{s-1}(\Omega) \backslash H^s(\Omega)$$

from Figure 4 on $\Omega = (0,1)^2$ with right-hand side $f \equiv -\Delta \mathbf{u}$ and $\nu = 1$.

Figure 5 shows the convergence history of the L^2 error for $s = 2$ and $s = 3$ for all three methods. The convergence speed clearly depends on the regularity of the solution and the employed reconstruction operator. For $s = 2$ the reconstruction with $\boldsymbol{\pi}^{\mathrm{BDM}}$ leads to better results and, more importantly, to a better convergence rate than the reconstruction with $\boldsymbol{\pi}^{\mathrm{RT}}$. For $s = 3$ the results show similar but milder differences between the two reconstructions. As predicted by Theorem 2, the reconstruction with $\boldsymbol{\pi}^{\mathrm{BDM}}$ leads to an optimal L^2 error convergence rate, while the Raviart-Thomas reconstruction $\boldsymbol{\pi}^{\mathrm{RT}}$ seems slightly suboptimal. Tables 10-15 show the computed values for all norms and allow similar conclusions for the other norms.

Since $p \equiv 0$, the results of the unmodified Crouzeix-Raviart method for $\boldsymbol{\pi}^{\mathrm{div}} = \boldsymbol{\pi}^{\mathrm{CR}}$ are the best. The benefits of the reconstructions in case of nonzero pressure can be seen in Examples 5.1 and 5.2 above.

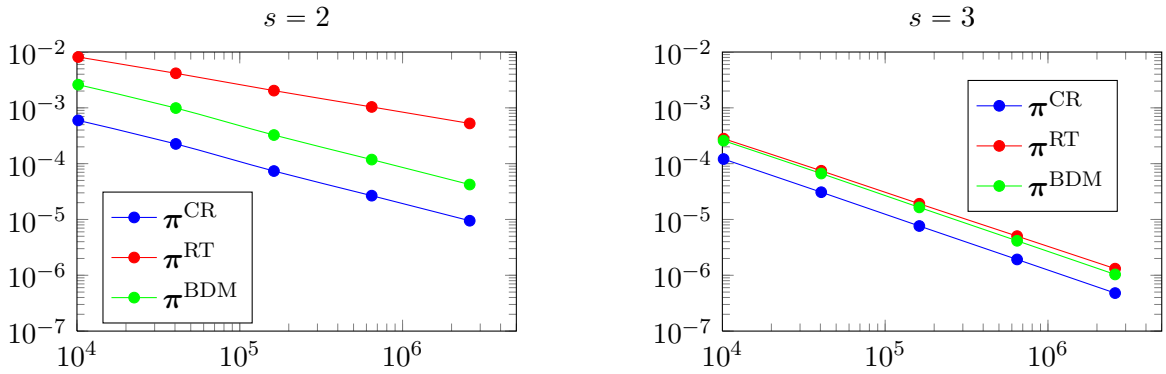

FIGURE 5. Convergence history of the L^2 error for the velocity in the benchmark problem of Section 5.4 for $s = 2$ (left) and $s = 3$ (right).

REFERENCES

[AD99] G. Acosta and R. G. Durán, *The maximum angle condition for mixed and nonconforming elements: application to the Stokes equations*, SIAM J. Numer. Anal. **37** (1999), no. 1, 18–36 (electronic). MR 1721268 (2000g:65107)

[BF91] Franco Brezzi and Michel Fortin, *Mixed and hybrid finite element methods*, Springer-Verlag New York, Inc., New York, NY, USA, 1991.

[BL08] E. Burman and A. Linke, *Stabilized finite element schemes for incompressible flow using Scott-Vogelius elements*, Appl. Numer. Math. **58** (2008), no. 11, 1704–1719. MR MR2458477 (2009k:65238)

[CGR12] Carsten Carstensen, Joscha Gedicke, and Donsub Rim, *Explicit error estimates for Courant, Crouzeix-Raviart and Raviart-Thomas finite element methods*, J. Comput. Math. **30** (2012), no. 4, 337–353. MR 2965987

[CR73] M. Crouzeix and P.-A. Raviart, *Conforming and nonconforming finite element methods for solving the stationary Stokes equations. I*, Rev. Française Automat. Informat. Recherche Opérationnelle Sér. Rouge **7** (1973), no. R-3, 33–75. MR 0343661 (49 #8401)

[DGT94] O. Dorok, W. Grambow, and L. Tobiska, *Aspects of finite element discretizations for solving the Boussinesq approximation of the Navier-Stokes Equations*, Notes on Numerical Fluid Mechanics: Numerical Methods for the Navier-Stokes Equations. Proceedings of the International Workshop

ndof	$\|\mathbf{u}-\mathbf{u}_h\|_0 \quad (\boldsymbol{\pi}^{\mathrm{CR}})$	$\|\mathbf{u}-\mathbf{u}_h\|_0 \quad (\boldsymbol{\pi}^{\mathrm{RT}})$	$\|\mathbf{u}-\mathbf{u}_h\|_0 \quad (\boldsymbol{\pi}^{\mathrm{BDM}})$
10176	5.957577e-04	8.132558e-03	2.596920e-03
40488	2.255780e-04	4.156489e-03	9.908448e-04
162152	7.371401e-05	2.033914e-03	3.255607e-04
646376	2.669053e-05	1.037216e-03	1.182694e-04
2585272	9.490658e-06	5.255378e-04	4.222973e-05

TABLE 10. L^2-error for the velocity in the benchmark problem of Section 5.4 for $s = 2$.

ndof	$\|\mathbf{u}-\mathbf{u}_h\|_{1,h} \quad (\boldsymbol{\pi}^{\mathrm{CR}})$	$\|\mathbf{u}-\mathbf{u}_h\|_{1,h} \quad (\boldsymbol{\pi}^{\mathrm{RT}})$	$\|\mathbf{u}-\mathbf{u}_h\|_{1,h} \quad (\boldsymbol{\pi}^{\mathrm{BDM}})$
10176	1.022823e-01	3.068302e-01	2.643498e-01
40488	7.803291e-02	2.286544e-01	1.946825e-01
162152	5.728900e-02	1.624617e-01	1.379248e-01
646376	4.316310e-02	1.185304e-01	9.954211e-02
2585272	3.223743e-02	8.573445e-02	7.160659e-02

TABLE 11. Energy error for the velocity in the benchmark problem of Section 5.4 for $s = 2$.

ndof	$\|p-p_h\|_0 \quad (\boldsymbol{\pi}^{\mathrm{CR}})$	$\|p-p_h\|_0 \quad (\boldsymbol{\pi}^{\mathrm{RT}})$	$\|p-p_h\|_0 \quad (\boldsymbol{\pi}^{\mathrm{BDM}})$
10176	1.698660e-02	1.327135e-01	5.455889e-02
40488	1.296949e-02	8.483679e-02	3.292390e-02
162152	8.127170e-03	4.549056e-02	1.994872e-02
646376	5.963909e-03	2.867073e-02	1.347808e-02
2585272	4.327458e-03	1.673502e-02	9.005974e-03

TABLE 12. L^2-error for the pressure in the benchmark problem of Section 5.4 for $s = 2$.

held at Heidelberg, October 1993, ed. by F.-K. Hebeker, R. Rannacher and G. Wittum **47** (1994), 50–61.

[FH88] L. Franca and T. Hughes, *Two classes of mixed finite element methods*, Computer Methods in Applied Mechanics and Engineering **69** (1988), no. 1, 89–129.

[GLBB97] J.-F. Gerbeau, C. Le Bris, and M. Bercovier, *Spurious velocities in the steady flow of an incompressible fluid subjected to external forces*, International Journal for Numerical Methods in Fluids **25** (1997), no. 6, 679–695 (Anglais).

[GR86] V. Girault and P.-A. Raviart, *Finite element methods for Navier-Stokes equations*, Springer Series in Computational Mathematics, vol. 5, Springer-Verlag, Berlin, 1986.

[JJRL14] E. Jenkins, V. John, L. Rebholz, and A. Linke, *On the parameter choice in grad-div stabilization for the stokes equations*, Advances in Computational Mathematics (2014), in press.

[Lin08] A. Linke, *Divergence-free mixed finite elements for the incompressible Navier-Stokes equation*, Ph.D. thesis, University of Erlangen, 2008.

[Lin09] ———, *Collision in a cross-shaped domain – a steady 2d navierstokes example demonstrating the importance of mass conservation in CFD*, Computer Methods in Applied Mechanics and Engineering **198** (2009), no. 41–44, 3278–3286.

[Lin14] Alexander Linke, *On the role of the Helmholtz decomposition in mixed methods for incompressible flows and a new variational crime*, Comput. Methods Appl. Mech. Engrg. **268** (2014), 782–800. MR 3133522

[OLHL09] M. A. Olshanskii, G. Lube, T. Heister, and J. Löwe, *Grad-div stabilization and subgrid pressure models for the incompressible Navier-Stokes equations*, Comput. Methods Appl. Mech. Engrg. **198** (2009), no. 49-52, 3975–3988. MR 2557485 (2010k:76070)

[OR04] M. Olshanskii and A. Reusken, *Grad-div stabilization for Stokes equations*, Math. Comp. **73** (2004), no. 248, 1699–1718.

[RT77] P.-A. Raviart and J. M. Thomas, *A mixed finite element method for 2nd order elliptic problems*, Mathematical aspects of finite element methods (Proc. Conf., Consiglio Naz. delle Ricerche

ndof	$\|\mathbf{u}-\mathbf{u}_h\|_0 \quad (\boldsymbol{\pi}^{\mathrm{CR}})$	$\|\mathbf{u}-\mathbf{u}_h\|_0 \quad (\boldsymbol{\pi}^{\mathrm{RT}})$	$\|\mathbf{u}-\mathbf{u}_h\|_0 \quad (\boldsymbol{\pi}^{\mathrm{BDM}})$
10176	1.209112e-04	2.801817e-04	2.579725e-04
40488	3.079067e-05	7.457767e-05	6.657434e-05
162152	7.635725e-06	1.911472e-05	1.645673e-05
646376	1.922028e-06	5.027921e-06	4.147565e-06
2585272	4.797008e-07	1.314357e-06	1.035006e-06

TABLE 13. L^2-error for the velocity in the benchmark problem of Section 5.4 for $s = 3$.

ndof	$\|\mathbf{u}-\mathbf{u}_h\|_{1,h} \quad (\boldsymbol{\pi}^{\mathrm{CR}})$	$\|\mathbf{u}-\mathbf{u}_h\|_{1,h} \quad (\boldsymbol{\pi}^{\mathrm{RT}})$	$\|\mathbf{u}-\mathbf{u}_h\|_{1,h} \quad (\boldsymbol{\pi}^{\mathrm{BDM}})$
10176	1.703294e-02	2.734736e-02	2.728000e-02
40488	8.619203e-03	1.395324e-02	1.394038e-02
162152	4.315794e-03	6.948807e-03	6.945189e-03
646376	2.168473e-03	3.489873e-03	3.488980e-03
2585272	1.085592e-03	1.745444e-03	1.745143e-03

TABLE 14. Energy error for the velocity in the benchmark problem of Section 5.4 for $s = 3$.

ndof	$\|p-p_h\|_0 \quad (\boldsymbol{\pi}^{\mathrm{CR}})$	$\|p-p_h\|_0 \quad (\boldsymbol{\pi}^{\mathrm{RT}})$	$\|p-p_h\|_0 \quad (\boldsymbol{\pi}^{\mathrm{BDM}})$
10176	4.014088e-03	4.655263e-03	4.575312e-03
40488	2.056652e-03	2.420779e-03	2.357163e-03
162152	1.027257e-03	1.173454e-03	1.161383e-03
646376	5.199862e-04	5.918578e-04	5.878378e-04
2585272	2.613183e-04	2.944506e-04	2.937313e-04

TABLE 15. L^2-error for the pressure in the benchmark problem of Section 5.4 for $s = 3$.

(C.N.R.), Rome, 1975), Springer, Berlin, 1977, pp. 292–315. Lecture Notes in Math., Vol. 606. MR 0483555 (58 #3547)

[Tem91] R. Temam, *Navier-Stokes equations*, Elsevier, North-Holland, 1991.